Soliton self-frequency shift: Self-similar solutions and their stability

Soliton self-frequency shift: Self-similar solutions and their stability

M. Facão*
Departamento de Física, Universidade de Aveiro, Campus Universitário de Santiago, 3810-193 Aveiro, Portugal

M. I. Carvalho†
DEEC/FEUP and INESCPorto, Universidade do Porto, Rua Dr. Roberto Frias, 4200-465 Porto, Portugal

D. F. Parker‡
School of Mathematics and Maxwell Institute for Mathematical Sciences, University of Edinburgh, The King's Buildings, Edinburgh EH9 3JZ, United Kingdom

(Received 21 July 2009; revised manuscript received 19 March 2010; published 20 April 2010)

Ultrashort pulse propagation in fibers is affected by intrapulse Raman scattering (IRS) which causes both a linear frequency downshift and a quadratic displacement of the peak pulse, as functions of the propagation distance. This effect has been known and treated by perturbation methods applied to the nonlinear Schrödinger equation since the period of intense research on soliton propagation. Here, we find solutions of the model equation using an accelerating self-similarity variable and study their stability. These solutions have Airy function asymptotics which give them infinite energy. For small IRS, the algebraically decaying tail is negligible and these solutions are a very good approximation of the profiles observed in the full equation simulations. For strong IRS (but beyond the regime in which the evolution equation is valid for silica fibers), the self-similar pulses have noticeable left tails exhibiting Airy oscillations. Whenever their truncated forms are used as initial conditions of the full equation, they experience amplitude decay and show left tails that are consistent with radiation escaping from the central pulse. These observations are interpreted as being the effects of a continuum constitution of the infinite left tail.

DOI: 10.1103/PhysRevE.81.046604 PACS number(s): 42.65.Tg, 42.81.Dp, 42.65.Dr

I. INTRODUCTION

Intrapulse Raman scattering is a nonlinear effect which must be considered in pulse propagation in fibers whenever the spectral width is sufficiently large that the material spectral Raman gain allows energy transfer from the high frequency to the low frequency components. The consequence of this phenomenon for the propagation of solitons in fibers is a continuous down-shift of the mean frequency of subpicosecond pulses. The effect was first observed in 1986 by Mitschke and Mollenauer [1], named as *soliton self-frequency shift* and, as demonstrated by Gordon [2], may be theoretically explained as a delayed Kerr response.

For spectral widths relatively small, the Raman gain spectrum may be approximately modeled by a linear function and the dimensionless evolution equation reads [3,4]

$$iq_Z + \frac{1}{2}q_{TT} + |q|^2 q = T_r(|q|^2)_T q, \tag{1}$$

where q is related to the complex amplitude of the optical field envelope by

$$q(Z,T) = \sqrt{\frac{\omega_0 n_2 \tau_0^2}{cA_{\text{eff}}|k''|}} A(z,\tau)$$

and the normalized distance and time are

$$Z = \frac{z|k''|}{\tau_0^2} \quad \text{and} \quad T = \frac{\tau}{\tau_0},$$

where $A(z,\tau)$ is such that $|A|^2$ represents the optical power and τ is measured in a reference frame that moves with the group velocity of the carrier frequency. The normalized Raman parameter is $T_r = t_r/\tau_0$, A_{eff} is the effective core area of the fiber, k'' is the group dispersion at the carrier frequency ω_0, c is the vacuum speed of light, n_2 is the Kerr coefficient and τ_0 is a normalization time.

Straightforward application of an adiabatic perturbation technique to the above perturbed nonlinear Schrödinger (NLS) equation yields a frequency shift given by [2]

$$\Delta\omega_0(z) = 5.12\frac{|k''|t_r}{t_{\text{fwhm}}^4} z,$$

where t_{fwhm} stands for the full width at half maximum in real units. The above result is in satisfactory agreement with the experimentally observed self-frequency shift. The factor t_{fwhm}^{-4} shows that the effect can be very large for pulse widths of a few tens of femtoseconds, however, it becomes negligible for pulse widths of several tens of picoseconds. As the group velocity is frequency dependent, this frequency shift also changes the soliton velocity from its original value and produces a temporal displacement of the pulses according to $2.56\ t_r t_{\text{fwhm}}^{-4} z^2$. These results anticipate that self-similar accelerating pulses might exist, as we will investigate in section II and which will generalize the procedure already applied to Eq. (1) in [5]. The stability of these pulses will be investigated using the Evans function method for the solutions to

*mfacao@ua.pt
†mines@fe.up.pt
‡d.f.parker@ed.ac.uk

which the method is applicable. Then, the obtained self-similar solutions will be used as input pulses of the simulation of the full evolution equation in order to complete the stability analysis. Finally, the conclusions are presented in Sec. IV.

II. SELF-SIMILAR SOLUTIONS

The temporal pulse displacement proportional to z^2 suggests the existence of a self-similar variable given by $\eta = T - \frac{a}{4}Z^2 + bZ$ (with a and b constants), as for screening photorefractive solitons [6]. Inserting the *ansatz* $q(Z,T) = \exp[i\theta(Z,\eta)]W(\eta)$, where both $\theta(Z,\eta)$ and $W(\eta)$ are real, into Eq. (1), we obtain

$$-\theta_Z W - \theta_\eta\left(b - \frac{a}{2}Z\right)W + \frac{1}{2}(W'' - \theta_\eta^2 W) + W^3 - 2T_r W^2 W' + i\left(b - \frac{a}{2}Z\right)W' + \frac{i}{2}(\theta_{\eta\eta}W + 2\theta_\eta W') = 0. \quad (2)$$

Both real and imaginary parts should vanish. Multiplying the imaginary part of the above equation by $2W$ and integrating in η, we obtain

$$\theta_\eta = \frac{a}{2}Z - b + \frac{B(Z)}{W^2},$$

where $B(Z)$ is the integration constant. Another integration in η yields

$$\theta(Z,\eta) = \left(\frac{a}{2}Z - b\right)\eta + E(Z) + B(Z)\int \frac{d\eta'}{W^2},$$

where $E(Z)$ is another integration constant. Using the above result for $\theta(Z,\eta)$ in the equation for the real part, we obtain

$$W'' + \left\{-a\eta - 2E'(Z) - 2B'(Z)\int \frac{d\eta'}{W^2} + \left(\frac{a}{2}Z - b\right)^2 - \frac{B^2(Z)}{W^4} + 2W^2 - 4T_r WW'\right\}W = 0. \quad (3)$$

Since W is not a function of Z, we assume $B(Z) = B = \text{const.}$ and impose that

$$-2E'(Z) + \left(\frac{a}{2}Z - b\right)^2 = -D = \text{const.} \quad (4)$$

These yield the following ordinary differential equation (ODE) for $W(\eta)$

$$W'' + \{-a\eta - D + 2W^2 - B^2W^{-4} - 4T_r WW'\}W = 0. \quad (5)$$

and integration of Eq. (4) in Z yields the following expression for θ

$$\theta(Z,\eta) = \left(\frac{1}{2}aZ - b\right)\eta + \frac{1}{2}(D + b^2)Z - \frac{1}{4}baZ^2 + \frac{1}{24}a^2Z^3 + \Phi(\eta), \quad (6)$$

with $W^2\Phi'(\eta) = B$. Equation (5) admits accelerating solutions ($a \neq 0$) having $W \to 0$ and $\Phi'(\eta) \neq \infty$ as $\eta \to \infty$ only for $B = 0$ and for $T_r \neq 0$. In turn, this implies that $\Phi(\eta) = \Phi = \text{const.}$ Furthermore, the two parameters a and T_r may then be replaced by a single parameter γ through the transformation

$$W(\eta) = \frac{\gamma}{4T_r}P(\zeta), \quad \zeta = \frac{\gamma}{4T_r}\eta, \quad \gamma = a^{1/4}(4T_r)^{3/4}, \quad (7)$$

from which results the following ODE

$$P'' + [-C - \gamma\zeta + 2P^2 - \gamma PP']P = 0, \quad (8)$$

where $C = D(4T_r/\gamma)^2$ is an arbitrary parameter.

We are interested in pulse solutions to Eq. (8) which describe stationary accelerating solutions to the full evolution equation. For such pulse solutions, the asymptotic behavior in the tails should match to the behavior of the Airy functions $\mathrm{Ai}(x)$ and $\mathrm{Bi}(x)$ since these form a basis for the solutions to the linearization of

$$R''(x) - xR + 2\gamma^{-2/3}R^3 - \gamma^{2/3}R^2R' = 0, \quad (9)$$

which is obtained by transforming Eq. (8) using

$$P(\zeta) \equiv R(x) \quad \text{with} \quad x \equiv \gamma^{1/3}\zeta + \gamma^{-2/3}C. \quad (10)$$

As $x \to +\infty$, $\mathrm{Ai}(x)$ tends exponentially to zero while $\mathrm{Bi}(x)$ grows exponentially. As $x \to -\infty$, both $\mathrm{Ai}(x)$ and $\mathrm{Bi}(x)$ have algebraically decaying oscillations of the same amplitude but differing in phase by $\pi/2$, namely,

$$\mathrm{Ai}(x) \sim \pi^{-1/2}(-x)^{-1/4}\sin\left(\frac{2}{3}(-x)^{3/2} + \frac{\pi}{4}\right),$$
$$\mathrm{Bi}(x) \sim \pi^{-1/2}(-x)^{-1/4}\cos\left(\frac{2}{3}(-x)^{3/2} + \frac{\pi}{4}\right). \quad (11)$$

Thus, as $x \to +\infty$, the pulse solutions $R(x)$ should tend to the form $c\,\mathrm{Ai}(x)$, while as $x \to -\infty$ they should tend to *any* solution $c_1\mathrm{Ai}(x) + c_2\mathrm{Bi}(x)$ to the Airy equation $R'' - xR = 0$.

Even though there is no analytical form for the pulse solutions of Eq. (8), for small γ we may arrive to an approximate solution using a perturbation approach. Hence, let us expand the solution $P(\zeta)$ whose peak is located at $\zeta = \zeta_0$ in powers of γ as

$$P(\zeta) = G(\zeta - \zeta_0) + \gamma P_1(\zeta) + \cdots. \quad (12)$$

Inserting the above expansion into Eq. (8), the leading order yields

$$P'' - CP + 2P^3 = 0,$$

for which the localized solitary solutions are $P(\zeta) = G(\zeta - \zeta_0) \equiv \sqrt{C}\,\mathrm{sech}[\sqrt{C}(\zeta - \zeta_0)]$, with $\zeta = \zeta_0$ being the (arbitrary) peak position. This sech solution is unsurprising since the case $T_r = 0$ and $a = 0$ reduces the evolution Eq. (1) to the NLS equation and our *ansatz* to its traveling solution. Then, taking the terms $O(\gamma)$ yields for $P_1(\zeta)$ the differential equation

$$P_1'' + (-C + 6G^2)P_1 = \zeta G + G^2G',$$

or, equivalently,

$$\frac{d^2P_1}{d\xi^2} + (6S^2 - 1)P_1 = C^{-1}(C^{1/2}\zeta_0 + \xi)S - CS^3T,$$

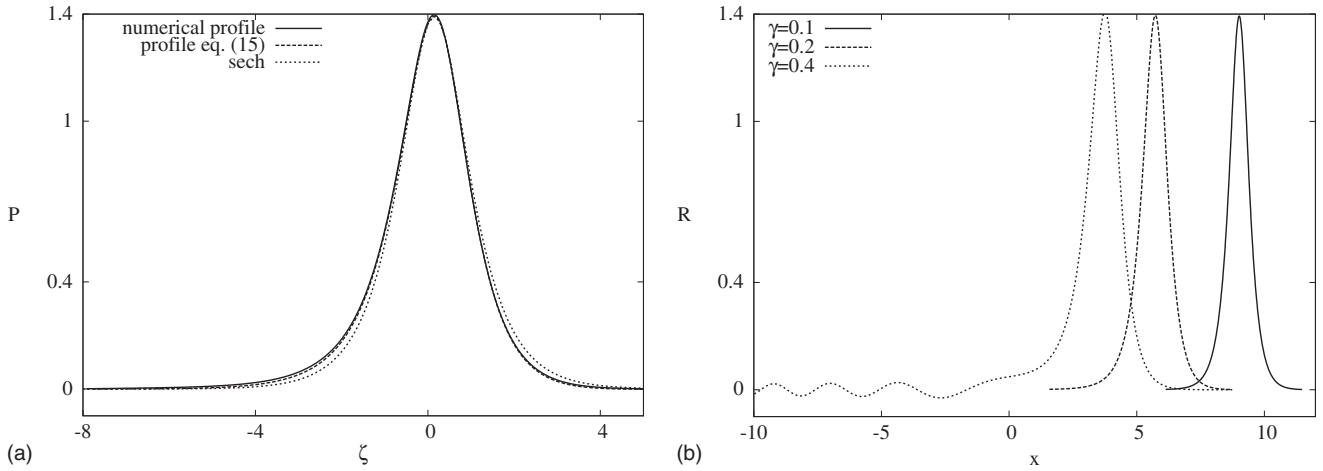

FIG. 1. (a) Comparison of the numerical $P(\zeta)$ for $\gamma=0.25$ and $\hat{P}$ from Eq. (15) and a sech profile. (b) Pulse profiles $R(x)$ for $\gamma=0.1$, 0.2 and 0.4.

$$\text{where} \quad S \equiv \operatorname{sech}\xi, \quad T \equiv \tanh\xi \tag{13}$$

with $\xi \equiv \sqrt{C}(\zeta-\zeta_0)$. Since the related homogeneous equation is self-adjoint and its only bounded solutions are multiples of $G'(\zeta-\zeta_0)$, the condition that Eq. (13) has bounded solutions is $\int_{-\infty}^{\infty}(\zeta G+G^2G')G'd\zeta=0$, which gives

$$C=\sqrt{15/4} \quad \text{with} \quad \zeta_0 \ \text{arbitrary}. \tag{14}$$

The bounded solution to Eq. (13) may be obtained by the method of reduction of order and is given by

$$P_1 = c_1 ST + \frac{1}{2\sqrt{C}}\zeta S - \frac{1}{4}\zeta^2 ST + \frac{C}{5}ST\ln(S),$$

which is an odd function if $\zeta_0=0$ and additionally can be made to have $P_1'(\zeta_0)=0$ through the *choice* $c_1=-(15)^{-1/2}$. With these choices, correct to order $O(\gamma)$, the pulse peak location approximately coincides with $\zeta=\zeta_0=0$ and the peak amplitude is $P(0)\cong\sqrt{C}$.

Based on the above perturbation approach we expect that for $\gamma \ll 1$ there exists an accelerating pulse $P(\zeta)$ given by

$$P(\zeta) \approx \hat{P}(\zeta) \equiv \sqrt{C}S + \gamma\left(-\frac{1}{2C}ST + \frac{1}{2\sqrt{C}}\zeta S - \frac{1}{4}\zeta^2 ST + \frac{C}{5}ST\ln(S)\right), \tag{15}$$

where S and T are the above functions with $\zeta_0=0$. Figure 1(a) shows $\hat{P}(\zeta)$ as given by Eq. (15) for $\gamma=0.25$. It is interesting to verify that no oscillations are predicted by Eq. (15), even though they are associated with the Airy functions for $x<0$. Thus, we anticipate that, for small γ, the pulse solution to Eq. (8) is well localized in the positive x semiaxis (that is, in $\zeta>-C/\gamma$), so that the tail decay is exponential like $\mathrm{Bi}(x)$ $(x>0)$ to the left and like $\mathrm{Ai}(x)$ to the right.

The pulse solutions to Eq. (8) can also be numerically determined. In order to do so, we devise a shooting method which starts by using location estimates from $G(\zeta)$. Therefore, we choose a suitably small value ϵ and use the values $\zeta_1=-C^{-1/2}\ln(2\sqrt{C}/\epsilon)$ and $\zeta_2=C^{-1/2}\ln(2\sqrt{C}/\epsilon)$ as first estimates for the locations at which $P(\zeta_1)=\epsilon$ and $P(\zeta_2)=\epsilon$. Then, from $\zeta=\zeta_2$ we integrate Eq. (8) backward with the following initial conditions:

$$P(\zeta_2) = R(x_2) = c\,\mathrm{Ai}(x_2) = \epsilon,$$

$$P'(\zeta_2) = \gamma^{1/3}R'(x_2) = c\gamma^{1/3}\mathrm{Ai}'(x_2),$$

where

$$x_2 \equiv \gamma^{1/3}\zeta_2 + \gamma^{-2/3}C,$$

until we find a minimum for $P^2+C^{-1}(P')^2$ at some $\zeta=\bar{\zeta}_1 \approx \zeta_1$. Then ζ_2 is adjusted in order to minimize $P^2+C^{-1}(P')^2$ until it becomes as small as ϵ^2 (that we have chosen as 5×10^{-6}) for some $\bar{\zeta}_1<0$. A similar procedure may be applied to integrate forward from ζ_1 in the left tail and using the function $\mathrm{Bi}(x)$. Following the above shooting method, we were able to find pulse solutions for which the two integrations agree, for γ up to approximately 0.25 (Fig. 1). The peak amplitude is very close to $C^{1/2}=(15/4)^{1/4}$ and the profile $P(\zeta)$ is also very close to $\hat{P}(\zeta)$ of Eq. (15) as determined using the perturbation approach [Fig. 1(a)]. The later figure also compares the numerical profile with a sech profile which shows clearly the asymmetry that grows as γ grows. As expected, these pulses are well within the region of positive x and the decay to the right and left tails are exponential.

For $\gamma>0.25$, it is not possible to find pulses for which $P^2+C^{-1}(P')^2$ becomes as small as $\epsilon^2\sim5\times10^{-6}$. This is unsurprising, since in this case we have $R(0)\sim2\times10^{-3}$, which implies that the left tail enters the region of negative x (i.e., for $\zeta<-C/\gamma$) where the Airy functions become algebraically decaying and oscillatory. However, if we do not require $P^2+C^{-1}(P')^2$ to reach ϵ^2, the shooting routine finds real solutions which decay algebraically to the left tail and exhibit observable Airy oscillations for $x<0$ [see profile for $\gamma=0.4$ in Fig. 1(b)]. As γ increases, the pulse peak becomes closer to $x=0$, the pulse is more asymmetric and the oscillations are larger in amplitude [Fig. 1(b)].

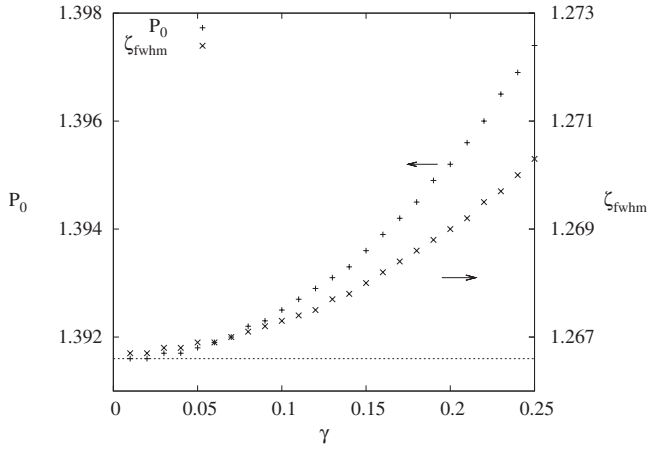

FIG. 2. Peak amplitude (represented by + and left y axis) and full width at half maximum (represented by $\times$ and right y axis) as function of γ. $\sqrt{C}$ (left y axis) and $1.76/\sqrt{C}$ (right y axis) are represented by the horizontal line.

We have analyzed the dependence of the amplitude and width of the profiles for which both tails decrease exponentially, i.e., solutions whose left tail starts to decay algebraically whenever is already very small. Figure 2 shows the peak amplitude P_0 and the full width at half maximum ζ_{fwhm} as a function of γ. There, small deviations of the peak value from $\sqrt{C}$ and ζ_{fwhm} from $1.76/\sqrt{C}$ are observable. Moreover, both increase with γ so that they do not follow the prediction $\zeta_{\text{fwhm}}=1.76/P_0$ which is characteristic of sech profiles.

Note that the strength of the intrapulse Raman effect is given by γ which may be written as $\gamma=4\zeta_{\text{fwhm}}t_r/t_{\text{fwhm}}$. Since the increase of ζ_{fwhm} is negligible, the effect increases with the magnitude of t_r and decreases with temporal width of pulses (increasing with spectral width). Apart from the asymmetry and the Airy tails arising for larger γ, the results obtained with self-similar solutions do not differ considerably from the results obtained with the perturbation about the NLS. The dependences of physical acceleration on t_{fwhm}/t_r as obtained by the two approaches are represented in Fig. 3.

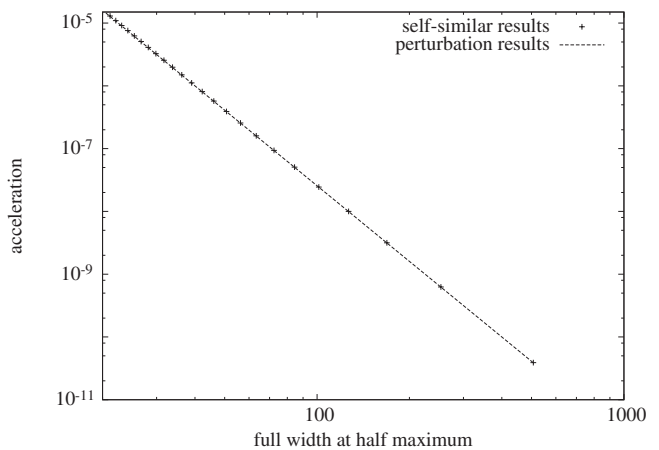

FIG. 3. Actual acceleration versus actual full width at half maximum, normalized by $|k''|^2/t_r^3$ and t_r, respectively. Points are obtained using the self-similar solution and the line represents the perturbation result.

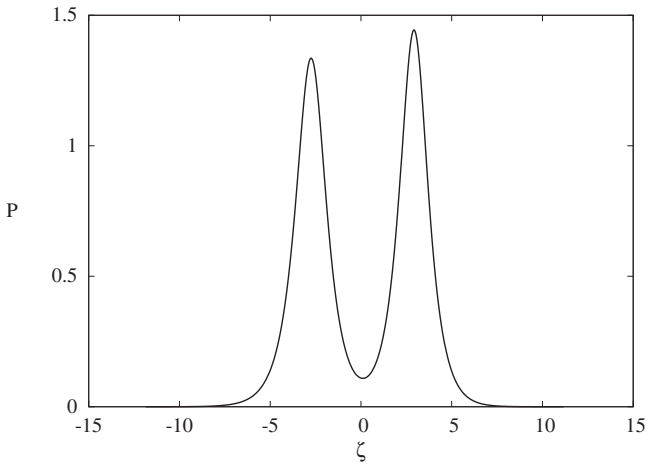

FIG. 4. Pulse profile $P(\zeta)$ with two humps for $\gamma=0.053$.

Our shooting procedure permits us to find multihumped profiles, as well. They exist in the same range of γ as the single-humped profiles and are centered around $\zeta=0$. They arise due to the nonautonomous character of Eq. (8). Figure 4 represents one example of these profiles that, in this case, has two peaks. These multihumped solutions do not propagate indefinitely without peak separation, however, the real distances during which they maintain their form may reach tens of meters, such that, they may be the precursors of the bound soliton pairs recently observed in photonic crystal fibers [7,8] as was further studied in [9].

III. STABILITY ANALYSIS

The stability of the accelerated solutions may be studied by the spectrum of the stability eigenvalue problem. To obtain it, we write a solution composed of the equilibrium $P(\zeta)$ plus a small complex perturbation $w(Z,\zeta)$, given by

$$q(Z,T) = \frac{\gamma}{4T_r}\exp[i\theta(Z,\zeta)][P(\zeta) + w(Z,\zeta)].$$

Introducing this solution into the evolution Eq. (1) and linearizing, we obtain

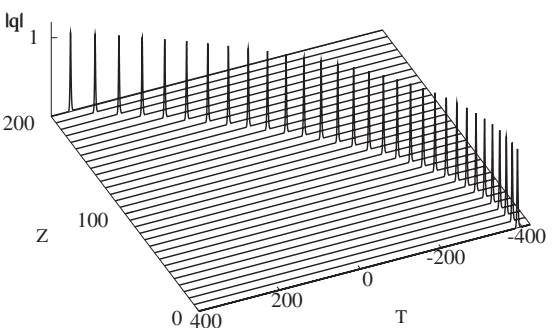

FIG. 5. Evolution along Z of self-similar profile for $\gamma=0.2$ and unitary peak amplitude.

$$2iw_{Z'} + w_{\zeta\zeta} - \frac{\gamma}{2}P^2(w_\zeta + w_\zeta^*) - \left(\gamma\zeta + C - 4P^2 + \frac{3\gamma}{2}PP'\right)w + \left(2P^2 - \frac{\gamma}{2}PP'\right)w^* = 0. \quad (16)$$

where $Z' = (\gamma/4T_r)^2 Z$. The stability eigenvalue problem is obtained from the above equation by considering that w depends exponentially upon Z' in the form $w(Z',\zeta) = u(\zeta)e^{i\lambda Z'} + v^*(\zeta)e^{-i\lambda^* Z'}$. Then the eigenvalue problem reads

$$L\begin{pmatrix} u \\ v \end{pmatrix} = \lambda\begin{pmatrix} u \\ v \end{pmatrix}, \quad (17)$$

where the operator L is given by

$$\begin{pmatrix} \frac{1}{2}\partial_{\zeta\zeta} - \frac{\gamma}{2}\zeta - \frac{C}{2} + 2P^2 - \frac{3\gamma}{4}PP' - \frac{\gamma}{4}P^2\partial_\zeta & P^2 - \frac{\gamma}{4}PP' - \frac{\gamma}{4}P^2\partial_\zeta \\ -P^2 + \frac{\gamma}{4}PP' + \frac{\gamma}{4}P^2\partial_\zeta & -\frac{1}{2}\partial_{\zeta\zeta} + \frac{\gamma}{2}\zeta + \frac{C}{2} - 2P^2 + \frac{3\gamma}{4}PP' + \frac{\gamma}{4}P^2\partial_\zeta \end{pmatrix}.$$

In the γ range such that the profiles decay exponentially in both tails, which was numerically observed for $\gamma \lesssim 0.25$, for ζ in the tails of $P(\zeta)$ the eigenvalue problem is equivalent to a decoupled pair of Airy equations. Following the arguments used in [6], we have applied a generalized Evans function method with Airy function asymptotics. We have not found any unstable eigenvalues using this methodology. For $\gamma \gtrsim 0.25$, the asymptotics of Eq. (17) are not really known since the decaying of the left tail of P is algebraic and as $\zeta \to -\infty$, there are other dominant terms than the Airy equation terms. In this range, it is not possible to apply the Evans function method.

The stability of the accelerating self-similar profiles was also evaluated by numerical simulation of the full evolution Eq. (1). Using the single-humped pulses as input, we obtained steady propagation with the expected acceleration (Fig. 5). However, the simulations up to $Z=300$ of a pulse with unit initial peak amplitude show that for $\gamma \gtrsim 0.25$ the peak amplitude decays with the propagation distance. This peak amplitude decay is plotted in Fig. 6. Since we are propagating pulses such that $q_{max} = W_{max} = 1$, the real distance is given by $z = 0.0037\ Z/\gamma^2$ (m) (we have used $t_r = 3$ fs and $|k''| = 20$ ps^2/km). Thus, $Z=300$ corresponds to a distance of 27.8 m for $\gamma=0.2$ and to 12.3 m for $\gamma=0.3$.

These simulations of the partial differential equation (PDE) also show that the profiles with Airy oscillations that we have obtained do not maintain their shape during propagation. Even though they evolve to pulses whose central part is identical to the input central part, they show a left tail whose modulus has no oscillations, although decays at the same rate as the Airy oscillations (Fig. 7). Although, the self-similar solution is an exact solution, the oscillatory Airy tails do not survive under the PDE numerical simulation, despite, they have been reported in a previous work [5]. In fact, the oscillations that were observed by [5] in their numerical simulation of the PDE may be due to their shorter propagation distance or even to reflection of the escaping radiation on the integration window limits. One fact that was not mentioned before is that the solutions having asymptotics like the Airy functions for negative x have infinite energy, so they are not allowed as physical solutions. Hence, the truncated self-similar solutions that are numerically used as input should adjust during propagation. The adjustment seems to

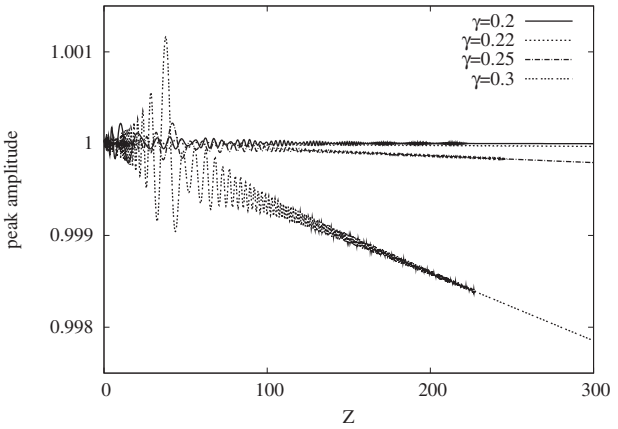

FIG. 6. Evolution along Z of peak amplitude of self-similar profiles.

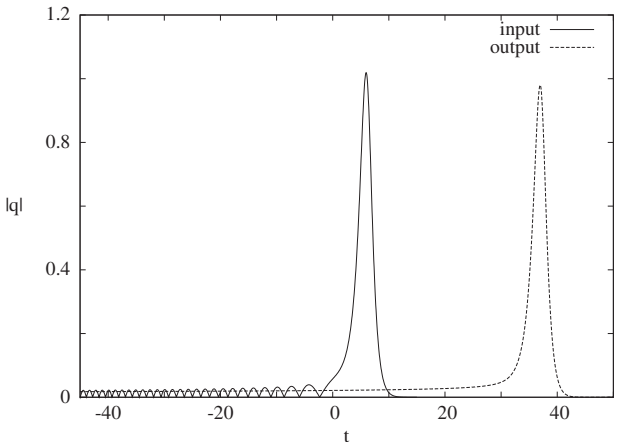

FIG. 7. Input (self-similar profile) and output for the PDE simulations corresponding to $\gamma=0.49$ ($T_r=0.17$ for unitary amplitudes).

require peak amplitude decay as is observed for $\gamma \gtrsim 0.25$ and Z up to 300, which suggests that our numerical propagating solitary waves behave like *radiatively decaying solitons* [10,11]. Indeed, it seems that energy is continuously and slowly escaping from the central pulse in order to complete what is in fault in the left tail. This also means that not all the initial energy is following the linear decrease in frequency of the accelerated pulse but instead stays as a higher frequency wing of the spectrum. Although a more accurate analysis should be performed to fully understand the dynamics of this small tail, its $(-x)^{-1/4}$ decay rate suggests that it is of the form $P(\zeta) \propto |\mathrm{Bi} + i\mathrm{Ai}|$. Actually, this type of solution has also been found in the context of a quantum wave equation for a charged particle under the potential of a constant electric field [12], a problem that shows some analogy with our stability problem (17) for small P.

Nevertheless, our simulations also show that, for $\gamma \lesssim 0.25$, the self-similar solutions are very much identical to the ones that propagate numerically so, probably, identical to the ones that propagate physically. Recall that for γ below 0.25, we have obtained steadily accelerating propagation for Z distances as large as 1000. For the particular value $\gamma = 0.2$, this Z corresponds to a real distance of 92.5 m. Note that for small γ, we surely have profiles that decay exponentially to the left tail, since we were able to obtain them by integration from the left using function Bi. Moreover, the oscillatory Airy tail should also be present in these profiles from $x=0$ to the left, however it is negligibly small for that the numerical truncation should not imply any observable adjustment. We have also propagated initial profiles given by $1.1P(\zeta)$ for which we observe that the pulse adjusts its shape and peak amplitude until it attains a steady propagation.

It is worthwhile to say that an identical self-similar variable was already used to describe the self-bending photorefractive solitons [6]. For them, the asymptotics were also of the Airy kind, however, the obtained profiles were away from the negative Airy x axis and well situated in the positive x region. Hence, whenever the tail entered the negative x region, it is already negligibly small, so that, every self-similar solution was a good approximation of the physical solution.

Fortunately, the limiting γ for which the self-similar solutions propagate steadily in the full equation almost coincides with the maximum value of γ such that Eq. (1) is a valid model for ordinary silica fibers. In fact, for silica fibers $t_r = 3$ fs [4] and the Eq. (1) describes the intrapulse Raman scattering for spectral widths less than the silica Raman gain peak at 13 THz, which imposes the bounds $t_{\mathrm{fwhm}}^{\mathrm{min}} = 65$ fs and $\gamma^{\mathrm{max}} = 0.235$. Hence, in the range of temporal widths for which our model is valid for silica fibers, the solutions are quite symmetrical, have very small Airy tails and propagate steadily.

IV. CONCLUSIONS

We have obtained self-similar accelerated solutions of the NLS plus intrapulse Raman scattering. These self-similar solutions have Airy function asymptotics which impose them infinite energy. Nevertheless, for relatively large pulses ($t_{\mathrm{fwhm}} \gtrsim 76$ fs), whose range almost coincides with the range of pulse widths for which this model is valid for silica fibers, these self-similar solutions are a very good approximation of the pulse profiles that propagate in the PDE simulator. They are well located in the positive Airy x semiaxis and have negligible Airy tails. For stronger IRS, which may be realized by shorter pulses or by larger Raman coefficient, the self-similar solutions are asymmetric and show an Airy left tail with pronounced oscillations. However, these oscillations do not survive in the PDE simulation. Moreover, we have observed that above approximately the same IRS strength ($\gamma \sim 0.25$) as the profiles start to show noticeable Airy tails (recall that the Airy tail amplitude is greater than 10^{-3} for $\gamma \gtrsim 0.25$), they propagate in the PDE simulator experiencing amplitude decay, which we interpreted as energy transference from the pulse to the incomplete tail. The escape of radiation from the central pulse to the left, in consistency with Airy function algebraic asymptotics, would also explain the observed form of the left tail. Hence, we consider that the accelerated self-similar solution is a very good approximation of the physical pulses propagating in silica fibers, however, a full analysis that includes radiation loss should be performed to recover the solutions that we have found in the simulation of the PDE, especially for large IRS.

ACKNOWLEDGMENT

We thank the referees for valuable suggestions that contributed to improve this paper.

[1] F. M. Mitschke and L. F. Mollenauer, Opt. Lett. **11**, 659 (1986).
[2] J. P. Gordon, Opt. Lett. **11**, 662 (1986).
[3] K. J. Blow and D. Wood, IEEE J. Quantum Electron. **25**, 2665 (1989).
[4] G. P. Agrawal, *Nonlinear Fiber Optics* (Academic Press, New York, 2001).
[5] N. Akhmediev, W. Królikowski, and A. J. Lowery, Opt. Commun. **131**, 260 (1996).
[6] M. Facão and D. F. Parker, Phys. Rev. E **68**, 016610 (2003).
[7] A. Podlipensky, P. Szarniak, N. Y. Joly, C. G. Poulton, and P. S. Russell, Opt. Express **15**, 1653 (2007).
[8] A. Podlipensky, P. Szarniak, N. Y. Joly, and P. S. J. Russell, J. Opt. Soc. Am. B **25**, 2049 (2008).
[9] M. Facão, M. I. Carvalho, and D. F. Parker, in Proceedings 11th International Conference on Transparent Optical Networks (2009), Vols. 1 and 2, pp. 390–393.
[10] J. P. Boyd, in *Advances in Applied Mechanics*, edited by J. W. Hutchinson and T. Y. Wu (Academic Press, New York, 1990), Vol. 27.
[11] P. Y. P. Chen and B. A. Malomed, Opt. Commun. **282**, 3804 (2009).
[12] R. Lefebvre, Int. J. Quantum Chem. **107**, 2643 (2007).